PASJ: Publ. Astron. Soc. Japan **55**, 433–444, 2003 April 25

Photon Emission in a Cascade from Relativistic Protons Initiated by Residual Thermal Photons in Gamma-Ray Bursts

Katsuaki ASANO and Fumio TAKAHARA
Department of Earth and Space Science, Osaka University, Toyonaka 560-0043
asano@vega.ess.sci.osaka-u.ac.jp, takahara@vega.ess.sci.osaka-u.ac.jp

(Received 2002 August 5; accepted 2003 February 20)

Abstract

Gamma-ray bursts are generally considered to be the result of internal shocks generated in an inhomogeneous relativistic outflow that arises from a fireball. In such shocks, the Fermi acceleration of protons is naturally expected to be at least as efficient as that of electrons. We investigate the consequences of proton acceleration in the residual thermal photon field of a fireball, especially those on the emission spectra of photons. In contrast to most other studies, we do not invoke a direct electron acceleration in shock waves. We show that the residual radiation field of the fireball can ignite the photopion production and subsequent cascade, and that the photons emitted in this process further enhance the photon-initiated cascade. We find that Fermi-accelerated protons with $\gtrsim 10^{13}$ eV efficiently bring their energy into pion production and subsequent photon emission. The particles cascading from the pions emit photons over a wide energy range. The photons emitted from electron–positron pairs distribute continuously from the GeV range down to the X-ray range, while muons can emit gamma-rays by synchrotron radiation with a break at around 1–10 MeV. We also discuss several radiation processes which may possibly produce a break feature in the MeV range, as observed in addition to muon synchrotron radiation.

Key words: gamma rays: bursts — non-thermal — radiation mechanisms: shock waves

1. Introduction

A widely accepted scenario for producing gamma-ray bursts (GRBs) is dissipation of the kinetic energy of a relativistic flow by relativistic shocks (see, e.g., a review by Piran 1999). The rapid time variabilities observed require that the GRB itself must arise from internal shocks within the flow, while the afterglow is due to external shock produced as the flow is decelerated upon collisions with the ambient medium. Although how the central engine of GRB produces the relativistic flow remains an open problem, the standard scenario is the high-entropy fireball scenario (Shemi, Piran 1990; Rees, Mészáros 1992; Mészáros, Rees 1993), in which a large amount of internal energy is injected into a compact region, such that the internal energy per one proton far exceeds the rest mass of the proton (Goodman 1986; Paczyński 1986). The huge internal energy of the fireball will be converted into the bulk kinetic energy of the relativistic flow, which we call the fireball wind. This fireball wind is accelerated to a relativistic velocity and the internal energy of the wind is finally dominated by baryonic matter. It is assumed that the fireball wind is inhomogeneous in order to produce internal shocks. The inhomogeneity in the wind may grow, and it ends up with multiple shells with different bulk Lorentz factors.

It is to be noted that protons carry a much larger amount of energy than electrons in the flow. In the standard GRB model, the observed spectra of GRBs are interpreted in terms of the synchrotron radiation emitted by relativistic electrons, which requires that a large fraction of the kinetic energy carried by protons is efficiently converted into that of relativistic electrons in the shocked region. However, this premise has not been theoretically proven. It is apparent that the Coulomb interaction cannot transport the internal energy of heated protons into electrons to achieve energy equipartition (Totani 1999), because the time scale of the Coulomb interaction is much longer than the dynamical time scale. As long as protons and electrons are accelerated independently in the shocked region, the total energy of accelerated protons should overweigh that of accelerated electrons by an order of their mass ratio. Although more efficient electron acceleration mechanisms in shocks may exist, at present no convincing one has been specified. On the other hand, efficient proton acceleration may lead to high-energy photon emission through photon-initiated cascades, as investigated in this paper. Even if we regard that efficient electron acceleration by shocks is quite possible, proton acceleration is naturally expected to be at least as efficient, and most probably more efficient; thus, the consequences of proton acceleration on photon spectra should be investigated.

One of the most important characteristics of GRB spectra is the existence of a typical break energy scale. The observed spectra of GRBs are approximated by a broken power law and the photon number spectra are approximated as $\sim \varepsilon_\gamma^{-2}$ above the break energy and $\sim \varepsilon_\gamma^{-1}$ below that. The apparent clustering of the break energy of GRB spectra in the 50 keV–1 MeV range (Preece et al. 2000) is an important key to understanding the physical processes in GRBs. Within the scheme of the standard model, the clustering of the break energy and the paucity of low energy photons below the break in GRB spectra (Preece et al. 1998, 2000) remain to be explained. The break energy scale has been conventionally adjusted by choosing the minimum energy of accelerated electrons. It is thus interesting to see if proton acceleration can provide other mechanisms to reproduce the break energy scale.

Although direct synchrotron emission from protons is too weak and too soft to reproduce GRBs for the expected values of the magnetic field, the emission from secondary particles is not safely neglected, provided that the Fermi-accelerated protons account for a large fraction of the internal energy and that there exist copious target photons to trigger the cascades. In order to optimistically estimate the high-energy neutrinos and extremely high-energy cosmic rays from GRBs, the Fermi-accelerated protons have often been assumed to have a large fraction of the internal energy. The physical conditions in GRBs imply that protons may be Fermi-accelerated to high energies (Waxman 1995). Waxman and Bahcall (1997) pointed out that a large fraction of the fireball energy is expected to be converted into high-energy neutrinos by photomeson production from the accelerated particles. In this paper, we explore the consequences of proton acceleration on the photon spectra and investigate if GRBs themselves are produced by proton acceleration.

Assuming that the accelerated protons account for a large fraction of the internal energy, we discuss the emission from particles produced in the cascades from high-energy protons. For simplicity and clarity, we assume that the energy density of directly accelerated electrons is very small compared to that of protons, so that the emission from this component is negligible in contrast to that found in almost all previous studies. In section 2, we argue that the residual radiation field of the fireball can trigger photopion production of relativistic protons. In section 3, the emission from the cascading particles is investigated. In section 4, we discuss the possibility to explain the observed spectral property of GRBs. Our conclusions are summarized in section 5.

2. Cascade Initiated by a Residual Radiation Field of the Fireball

In this section we discuss photopion production in the internal shock against residual thermal photons of the fireball. While most of previous studies have ignored the effects of the residual photons, we argue that this is not legitimate, and that these photons play an important role to trigger photopion production. The cascade triggered by the collisions of shock-accelerated protons with residual photons can efficiently transport the dissipated energy into electron–positron pairs. A schematic diagram of the energy transfer is shown in figure 1. In the following, we discuss the ignition of GRBs according to this diagram.

In order to discuss this issue, we need to specify the distribution of the residual radiation field. We regard that the central engine produces an inhomogeneous fireball wind for a long duration compared to the dynamical time scale of the central engine. The inner region of the fireball wind is optically thick and the radiation and matter in the fireball wind behaves like a single fluid moving with the same velocity. In the radiation-dominated stages, as the wind expands, the Lorentz factor of the wind increases in proportion to the radius (Piran et al. 1993). After the fireball wind becomes matter-dominated, the wind plasma coasts with a constant radial speed. The fireball wind becomes optically thin at the photospheric radius where matter and radiation decouple. We treat this decoupled radiation field as the residual radiation field.

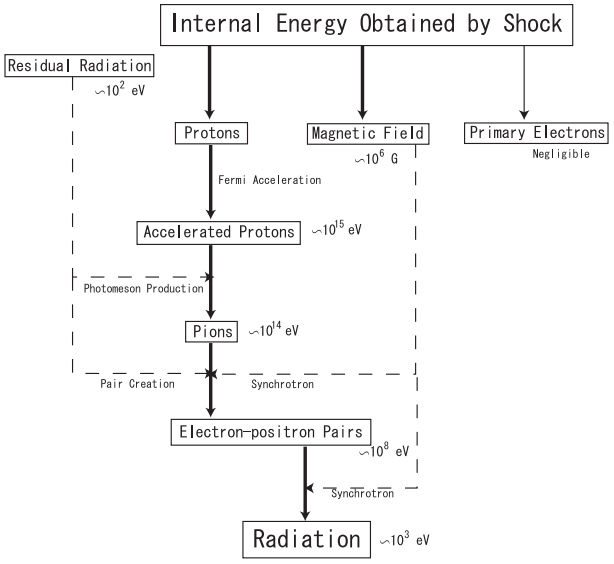

Fig. 1. Process of the cascade ignited by the residual radiation in the fireball (see section 2). We neglect the effects of direct electron acceleration. The solid arrows show the energy flow. The dashed arrows indicate the interactions that induce energy transfer to lower energy particles. The typical energies of each particle measured in the comoving frame are noted.

In the internal shock scenario, there exist inhomogeneities of the matter in the wind, and they end up with multiple shells with different bulk Lorentz factors. Internal shocks arise from collisions of the shells. As for the Lorentz factor of the shells, we follow the general constraints obtained in the conventional internal-shock scenario. The bulk Lorentz factor of the shells lies between one hundred and a few thousand (Mészáros, Rees 2000). Moreover, the energy-efficiency argument concerning the internal shock model requires a large dispersion of the Lorentz factor of individual shells (Kobayashi, Sari 2001; Guetta et al. 2001). Efficient dissipation of the kinetic energy is possible only when the difference in the Lorentz factors of the two colliding shells is sufficiently large. Thus, we regard that independent multiple shells are arising intermittently from the central engine to satisfy the required large dispersion of their Lorentz factors.

On the other hand, the inhomogeneity of the residual radiation field is less clear and the degree of inhomogeneities largely depends on the character of the central engine, about which we have little information. The residual photon field in the wind may not necessarily distribute discontinuously as do the matter shells. Therefore, we consider two extreme cases for the residual photon field (see figure 2). In one case, we assume that radiation is strongly coupled with matter and is contained in the shell. In this case, each shell is regarded to represent an independent fireball. We assume that there is no matter and radiation between the shells before the radiation field in a shell decouples with matter. In this case, we completely neglect the radiation field emitted from other shells. Hereafter, we call this case the "Discrete Model."

In the other extreme case, we assume that the photon field is given by a quasi-steady continuous wind, for which the effects

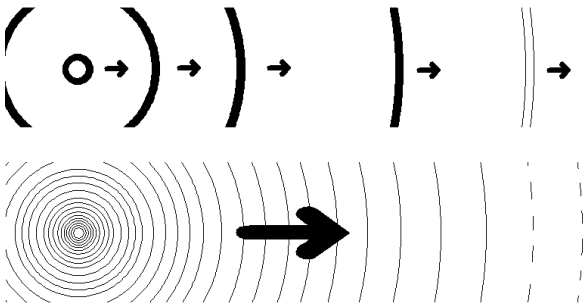

Fig. 2. Schematic representation for the Discrete Model (above) and the Continuous Model (below). The white shell (above) and the dashed lines (below) represent fluid outside of $R_{\rm ph}$.

of the inhomogeneities are neglected. Inside the photosphere the radiation and matter are considered to be continuously distributed and coupled with each other. Outside of the photosphere photons escape freely to infinity. In this case the radiation field behaves smoothly, as determined from the wind parameters. Even though this treatment formally neglects the inhomogeneities in the wind, in reality inhomogeneities should exist, and we assume that the internal shocks occur and high-energy protons are injected at some places in the radiation field. We do not discuss the detail of the internal shocks in this model. The latter case is called the "Continuous Model" hereafter.

For simplicity, we assume spherical symmetry for both models.

2.1. *Residual Photon Field*

2.1.1. *Discrete Model*

We first discuss the Discrete Model. We consider the situation where the inner faster shell overtakes the outer slower one and generates forward and reverse shocks in the respective shells. We suppose that the typical Lorentz factors of the faster and slower shells are $\Gamma_{\rm r} \sim 1000$ and $\Gamma_{\rm s} \sim 100$, respectively. Each shell is emitted from the central engine as a fireball with some initial radius Δ. Each fireball ends up as a coasting matter shell, retaining its width (Δ) in the observer frame. The radiation field in each shell evolves independently of other shells. In the initial radiation-dominated phase, the radiation energy density in the fireball behaves as $e \propto r^{-4}$ (r is the location of the shell), and the bulk Lorentz factor of the shell increases in proportion to r (Piran et al. 1993). After the shell enters the matter-dominated regime, as long as the shell is optically thick to scattering, the radiation energy density declines as $e \propto r^{-8/3}$ and the shell eventually coasts with $\Gamma = E/Mc^2$, where M and E are the total baryon rest mass and the total energy of the shell, respectively. Since there is no matter between shells in the Discrete Model, once a photon escapes from the shell, it moves freely.

In this case, the shell becomes optically thin at the radius

$$R_{\rm ph} = \sqrt{\frac{\sigma_{\rm T} M}{4\pi m_{\rm p}}}, \tag{1}$$

where $\sigma_{\rm T}$ is the Thomson cross section. The radius $R_{\rm ph}$ becomes 6×10^{12}–6×10^{13} cm for a range $Mc^2 = 10^{48}$–10^{50} erg. The kinetic energy of one shell which we consider corresponds to 10^{50}–10^{53} erg for $\Gamma = 100$–1000. Then, we obtain the temperature of the residual radiation field at $r = R_{\rm ph}$ in the shell rest frame as

$$T = 130(\Gamma_3 \Delta_7 M_{48})^{-1/12} \ \ {\rm eV}, \tag{2}$$

where $\Gamma_3 = \Gamma/10^3$, $\Delta_7 = \Delta/10^7$ cm, and $M_{48} = Mc^2/10^{48}$ erg. The parameter dependence of the temperature is very weak. The shell coasts $R_{\rm esc} \equiv 2\Gamma^2\Delta \simeq 2 \times 10^{13} \Delta_7 \Gamma_3^2$ cm from the radius $r = R_{\rm ph}$ before the residual photons escape from the shell. Thus, the energy density of residual photons in the comoving frame is as large as $10^{10}\,{\rm erg\,cm^{-3}}$ when the shell reaches a few times 10^{13} cm for $\Gamma = 10^3$.

The inner faster shell overtakes the outer slower one at $r \simeq \Gamma_{\rm s}^2 \delta$, where δ is the initial separation between the two shells in the observer rest frame. When δ is small enough, the collisions occur well inside of $R_{\rm ph}$ and no major observational feature is expected. For $\delta \simeq 10^9$ cm (which is consistent with the observed time variability of GRBs) and $\Gamma_{\rm s} \gtrsim 100$, the two shells collide outside of $R_{\rm ph} \simeq 10^{13}$ cm. The typical radius where the internal shocks occur can be comparable to $R_{\rm ph}$, unless the initial separation of two shells is limited to larger than 10^{10} cm. Since the collision radius is comparable to $R_{\rm esc}$ for the faster shell with $\Gamma_{\rm r} \simeq 10^3$, internal shocks can occur in the thermal radiation field in the faster shell with temperature $T \simeq 100$ eV. On the other hand, when δ is much larger than 10^{10} cm, internal shocks occur far outside of $R_{\rm ph}$ and the residual photons have already escaped from the shell. In this case there is no photon field in the shell when the internal shocks occur, which is not interesting for the present study. In the Discrete Model, therefore, we consider only the internal shocks that occur around the radius $r = R_{\rm ph}$. In the comoving frame the width of the shocked region in the outer shell is thinner than that of the inner shell when Δ and M of the two shells are similar to each other. Since the photons in the shocked region in the outer shell escape more promptly, we discuss only the reverse shocked region of the inner shell. Hereafter, we denote Γ_3 as the normalized Lorentz factor of the inner shell ($\Gamma_{\rm r} = 10^3 \Gamma_3$).

The internal shock is mildly relativistic, i.e., the Lorentz factor $\Gamma_{\rm R}$ of the reverse shock observed from the rest frame of the inner shell is a few. For example, when two shells with the same M and Δ collide with $\Gamma_{\rm s} = 100$ and $\Gamma_{\rm r} = 1000$, we have $\Gamma_{\rm R} = 2.57$. From the jump condition (Sari, Piran 1995), the shell width in the comoving frame of the shocked matter is $l = \Delta\Gamma_{\rm r}/(4\Gamma_{\rm R} + 3) \simeq 10^9 \Delta_7 \Gamma_3$ cm. Then, the internal energy density in the shocked shell at $r = R_{\rm ph}$ is obtained as

$$U_{\rm in}(R_{\rm ph}) = \frac{(\Gamma_{\rm R} - 1)Mc^2}{4\pi R_{\rm ph}^2 l} = \frac{(\Gamma_{\rm R} - 1)(4\Gamma_{\rm R} + 3) m_{\rm p} c^2}{\sigma_{\rm T} \Gamma_{\rm r} \Delta}$$
$$\simeq 10^{12} \Delta_7^{-1} \Gamma_3^{-1} \ \ {\rm erg\,cm^{-3}}, \tag{3}$$

where we have assumed $(\Gamma_{\rm R} - 1)(4\Gamma_{\rm R} + 3) \simeq 10$. Thus, the energy density of residual photons is about 1% of the internal energy of baryons.

In the internal or external shocks of GRBs strong magnetic fields should be produced, since the expected magnetic field frozen from the central engine is several orders of magnitude

smaller than the value required to produce gamma-rays because of the adiabatic expansion. Although no specific mechanism is widely accepted, the relativistic two-stream instability (Medvedev, Loeb 1999) is one of the candidates to generate such a high magnetic field. In this paper, we assume that the constant ratio ($f_{\rm B}$) of the internal energy ($U_{\rm in}$) goes into the magnetic field; then, the magnetic field at radius $R_{\rm ph}$ becomes

$$B(R_{\rm ph}) = \sqrt{8\pi f_{\rm B} U_{\rm in}} \simeq 2\times 10^6 \left(\frac{f_{\rm B}}{0.1}\right)^{1/2} \Delta_7^{-1/2}\Gamma_3^{-1/2}\ {\rm G}. \quad (4)$$

2.1.2. Continuous Model

Differently from the Discrete Model, for the Continuous Model we consider a quasi-steady fireball wind of total luminosity $L = 10^{52} L_{52}$ erg s^{-1} expanding from the initial radius Δ. Although the radiation and matter are assumed to be continuously distributed in the estimation of the distribution of the physical quantities, in reality build-in inhomogeneities can make the internal shocks occur somewhere and high-energy protons are injected. We do not deal with the details of the internal shocks in this model. The injected high-energy protons will interact with the continuous radiation field. The wind is characterized by the average baryon load parameter, $\eta \equiv L/\dot{M}c^2 = 100\eta_2$. The photosphere and photospheric temperatures in this case were well studied by Mészáros and Rees (2000). In the radiation-dominated region the bulk Lorentz factor of the wind increases as $\Gamma \propto r$ (r is the radial coordinate in this model). For relatively low values of $\eta < \eta_* \equiv (L\sigma_{\rm T}/4\pi m_{\rm p} c^3 \Delta)^{1/4} = 10^3 L_{52}^{1/4}\Delta_7^{-1/4}$, the increase of Γ stops at the saturation radius, $r_{\rm s} \equiv \eta\Delta$, and the flow continues to coast with $\Gamma = \eta$ above $r_{\rm s}$. In this paper we consider only this range of η. The photosphere is located at a radius

$$R_{\rm ph} = \frac{L\sigma_{\rm T}}{4\pi m_{\rm p} c^3 \Gamma^3} \simeq 10^{13} L_{52}\eta_2^{-3}\ {\rm cm}. \quad (5)$$

We obtain the radiation temperature at $r = R_{\rm ph}$ in the wind rest frame as

$$T = 40\eta_2^{5/3} L_{52}^{-5/12}\Delta_7^{1/6}\ {\rm eV}. \quad (6)$$

Although the representative numerical values of $R_{\rm ph}$ and T are similar to those of the Discrete Model, their parameter dependence is rather strong compared with the dependence in the Discrete Model. Outside of $R_{\rm ph}$, the radiation field is approximated by a diluted black body with temperature T. In the wind rest frame, the number density of the residual photons declines as r^{-2}. Although the energy density of residual photons is an order of magnitude smaller than that in the Discrete Model, the photon distribution is not limited in narrow shells, and they are available for a longer time scale.

The average total energy density in the wind rest frame, $U = L/4\pi r^2\eta^2 c$, is given by

$$U = \frac{4\pi m_{\rm p}^2 c^5 \eta^4}{L\sigma_{\rm T}^2}\left(\frac{r}{R_{\rm ph}}\right)^{-2} \quad (7)$$

$$\simeq 2\times 10^{10}\eta_2^4 L_{52}^{-1}\mathcal{R}^{-2}\ {\rm erg\,cm^{-3}}, \quad (8)$$

where $\mathcal{R} \equiv r/R_{\rm ph}$. If the fraction $f_{\rm B}$ of U goes into the magnetic field, it becomes

$$B = 2\times 10^5 \left(\frac{f_{\rm B}}{0.1}\right)^{1/2} \eta_2^2 L_{52}^{-1/2}\mathcal{R}^{-1}\ {\rm G}. \quad (9)$$

These values are for a continuous wind, and the effects of inhomogeneities are not taken into account. When an inhomogeneity causes an internal shock which propagates in the background wind flow, the internal energy and magnetic field can be larger than the values given in equations (8) and (9) locally. However, for simplicity, in the following numerical estimation we do not consider such factors in the Continuous Model. The dynamical time scale in the Continuous Model is taken to be $r/c\eta$, which is typically two orders of magnitude longer than that in the Discrete Model (l/c).

2.2. Photopion Production by Accelerated Protons

The maximum energy of accelerated protons is estimated from the conditions that the cooling time of protons should be longer than the Fermi acceleration time scale, and that the Larmor radius should be smaller than the shell width. For the Discrete Model, the maximum energy of protons at $r = R_{\rm ph}$ is most likely determined by the latter condition when $f_{\rm B} \ll 1$. For $f_{\rm B} = 0.1$ and $l = 10^9$ cm, however, both of the conditions give comparable values of the maximum energy, which turn out to be $\sim 10^{17}$ eV. For the Continuous Model, a similar value of the maximum energy is obtained. The accelerated protons would obey a power-law distribution and may account for a large fraction of the internal energy. The thermal photons interact with these protons to produce photopions.

Although in the shocked fluid rest frame the residual photons undergo a red-/blue-shift and their distribution becomes anisotropic, an isotropic distribution is a quite good approximation in a relativistic flow. Thus, we neglect the anisotropy and suppose that the accelerated protons interact with the isotropic thermal radiation field with a given temperature. The typical Lorentz factor of accelerated protons that interact resonantly with the thermal photons is $\gamma_{\rm p,typ} = \varepsilon_{\rm th}/T$, where $\varepsilon_{\rm th} \simeq 145$ MeV is the threshold energy of a photon in the proton rest frame.

2.2.1. Discrete Model

For the Discrete Model, we consider the internal shocks that occur around the radius $r = R_{\rm ph}$. The typical energy of pion producing protons becomes $E_{\rm p,typ} \simeq 10^{15}$ eV for $T = 100$ eV. At $r = R_{\rm ph}$ the number density of the photons is written as

$$n(\varepsilon_\gamma) = \frac{8\pi}{(hc)^3}\frac{\varepsilon_\gamma^2}{\exp(\varepsilon_\gamma/T) - 1}. \quad (10)$$

The time scale of photopion production, t_π, is written as

$$t_\pi^{-1}(\gamma_{\rm p}) = 2\pi c \int_0^\pi d\theta \sin\theta(1-\cos\theta) \times \int_{\varepsilon'_{\rm th}}^\infty d\varepsilon_\gamma \frac{n(\varepsilon_\gamma)}{4\pi}\sigma_\pi(\chi), \quad (11)$$

where θ is the incident angle between the two interacting particles. We approximate the photopion production cross section (e.g. Stecker 1968) by a broken power-law profile as $\sigma_\pi(\chi) = 5\times 10^{-28}(\chi/590)^{3.2}$ cm^2 for $290 < \chi < 590$ and $\sigma_\pi(\chi) = 5\times 10^{-28}(\chi/590)^{-0.7}$ cm^2 for $590 < \chi < 9800$, where $\chi m_{\rm e} c^2$ is the photon energy in the proton rest frame. In

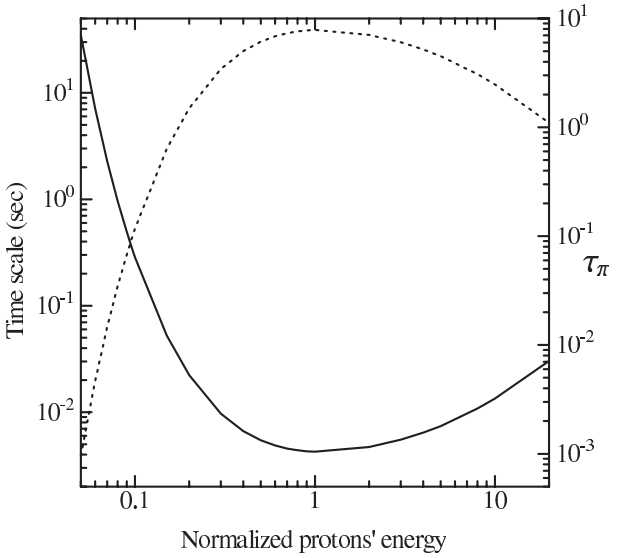

Fig. 3. Time scale (solid line) and τ_π (dotted line) of protons for photopion production in the thermal photon field. The time scale $t_{\mathrm{p},\pi} \propto T^{-3}$ and the optical depth $\tau_\pi \propto t_{\mathrm{p},\pi}^{-1} l$. We assume $T = 100$ eV and $l = 10^9$ cm in this figure. The protons' energy is normalized by $E_{\mathrm{p,typ}} = m_\mathrm{p} c^2 \varepsilon_\mathrm{th}/T$.

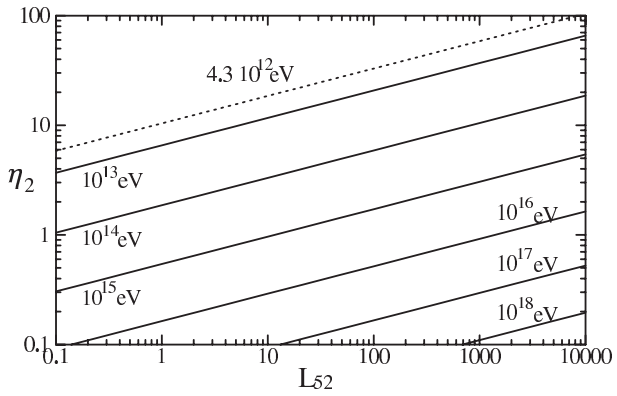

Fig. 4. Threshold energy of the photopion production, $E_{\mathrm{p},\tau}$, at the photosphere in the Continuous Model for $\Delta_7 = 1$. The dotted line corresponds to $\eta = \eta_*$.

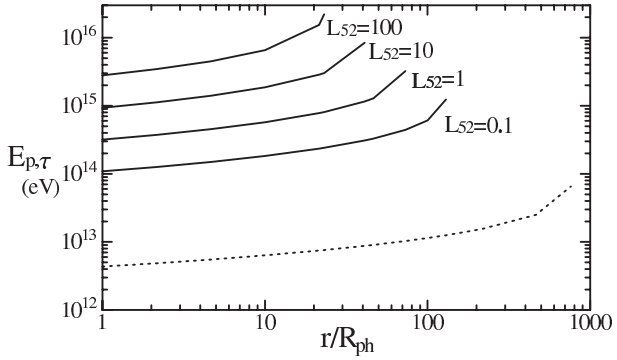

Fig. 5. Threshold energy, $E_{\mathrm{p},\tau}$, for $\eta_2 = 1$ and $\Delta_7 = 1$ against r in the Continuous Model. The dotted line is the same as in figure 4.

the fluid rest frame the energy of a photon is expressed as $\varepsilon_\gamma = \chi m_\mathrm{e} c^2/\gamma_\mathrm{p}(1-\cos\theta)$. Since the residual photons escape in the dynamical time scale l/c, we regard that efficient pion production occurs if t_π is less than l/c. In figure 3, we plot the time scale t_π and $\tau_\pi \equiv t_\pi^{-1} l/c$ for the photopion production in the 100 eV radiation field. It is seen that for $E_\mathrm{p} = E_{\mathrm{p,typ}} \simeq 10^{15}$ eV τ_π becomes $\sim 8(l/10^9\,\mathrm{cm})$, which means that efficient pion production occurs. The threshold energy of protons for pion production, $E_{\mathrm{p},\tau}$, at which τ_π becomes one, is 2×10^{14} eV for $T = 100$ eV. Therefore, protons with 10^{14}–10^{17} eV efficiently produce π^0s and $\pi^\pm$s. The photopion production would not occur outside of a few times R_ph because the photon number density decreases as $\tau_\pi \propto r^{-2}$, even if the residual photon field remains in the shell. Since the average inelasticity is about 20%, the typical energy of produced pions should be 10^{13}–10^{16} eV.

2.2.2. *Continuous Model*

When an internal shock occurs in a continuous wind, the accelerated protons will be injected into the wind. The accelerated protons can interact with photons during much longer period of time ($r/c\eta$) than in the Discrete Model (l/c). In figure 4 we plot the threshold energy, $E_{\mathrm{p},\tau}$, at the photosphere calculated numerically in a similar way to that in the Discrete Model. The energy $E_{\mathrm{p},\tau}$ weakly depends on L_{52}. The dotted line in figure 4 corresponds to $\eta = \eta_*$, the maximum value allowed for the saturated fireball wind. For fiducial values of $\eta_2 = 1$ and $L_{52} = 1$, the threshold energy becomes 3×10^{14} eV, which is almost the same as the typical value for the Discrete Model. Thus, in the Continuous Model, too, efficient photopion production occurs around the photosphere.

This may be understood qualitatively as follows. Because τ_π is a steeply increasing function of the energy in the low-energy range, as can be seen in figure 3, the threshold energy is roughly taken as a fixed fraction of the typical energy for photopion production, which is inversely proportional to the photon temperature. Since $\tau_\pi(E_{\mathrm{p,typ}}) \propto T^3 R_\mathrm{ph}/\eta$, we may approximate $E_{\mathrm{p},\tau} \propto E_{\mathrm{p,typ}} \propto \eta_2^{-5/3} L_{52}^{5/12}$. It is seen that this simple relation well reproduces the plots in figure 4.

Since in the Continuous Model the residual photons distribute continuously, the photopion production can occur even outside of R_ph. In figure 5, we show the threshold energy, $E_{\mathrm{p},\tau}$, against r for $\eta_2 = 1$. Although the value τ_π drops as $\propto r^{-1}$, $E_{\mathrm{p},\tau}$ itself does not increase drastically. The region where efficient photopion production can occur by the thermal radiation field is inside of $r \simeq 100 R_\mathrm{ph}$. Therefore, we expect a large fraction of the energy of protons ($\gtrsim 10^{14}$ eV for $L_{52} \simeq 1$) to efficiently go to the energy of pions.

In the Discrete Model we have assumed that the internal shocks occur near $r = R_\mathrm{ph}$. Therefore, the physical conditions in the shocked region are somewhat restricted. On the other hand, in the Continuous Model, photopion production occurs over a wide range of r and the properties of the photon emission may depend on the parameters η, L, and $\mathcal{R}$. For simplicity, we describe the emission from the cascading particles mainly along the Discrete Model below, while the Continuous Model is briefly mentioned. As will be shown later, however, there are no drastic differences in the results between the two Models.

2.3. Behavior of Pions

The created π^0s decay immediately into two gamma-rays, which are converted into electron–positron pairs, while the minor portion directly escapes from the shocked region. The fate of these high-energy photons is discussed in the next subsection. On the other hand, the lifetime of most $\pi^{\pm}$s ($E_\pi \gtrsim 0.2E_{\rm p,typ} \simeq 2\times10^{14}$ eV) is longer than the dynamical time scale $l/c \simeq 0.03$ s for the Discrete Model because of the large Lorentz factor. The energy density of residual photons is about $10^{10}\,{\rm erg\,cm^{-3}}$, which is smaller than the energy density of the magnetic field if B is larger than 5×10^5 G. Thus, synchrotron loss is the dominant cooling process for the charged pions.

The synchrotron cooling time scale of $\pi^{\pm}$ is expressed as

$$t_{\pi,\rm cool} = \frac{6\pi m_\pi^3 c}{\sigma_{\rm T} m_{\rm e}^2 B^2 \gamma_\pi} \simeq 2\times10^{-3}\left(\frac{f_{\rm B}}{0.1}\right)^{-1}\left(\frac{E_\pi}{2\times10^{14}\,{\rm eV}}\right)^{-1}\Delta_7\Gamma_3\ {\rm s}, \quad (12)$$

where γ_π is the Lorentz factor of pions. The cooling time of high-energy pions becomes shorter than their lifetime. The lifetime of pions becomes comparable to the cooling time for

$$\gamma_\pi^2 = \frac{6\pi m_\pi^3 c}{\sigma_{\rm T} m_{\rm e}^2 B^2 t_{\pi,0}} \equiv \gamma_{\pi^0}^2, \quad (13)$$

where $t_{\pi,0} = 2.6\times10^{-8}$ s is the lifetime of pions in the rest frame. Thus, charged pions ($E_\pi \gtrsim 2\times10^{14}$ eV) cool down to $m_\pi c^2\gamma_{\pi^0} = 5\times10^{13}(f_{\rm B}/0.1)^{-1/2}$ eV before they decay into muons. Charged pions with lower energies decay into charged muons before significant cooling, and most of their energy is converted into photons by synchrotron radiation because the lifetime of charged muons is much longer than that of charged pions.

The energy of the synchrotron photons emitted by charged pions is

$$\varepsilon_\pi = \frac{\hbar q B}{m_\pi c}\gamma_\pi^2 \sim 9\times10^7\left(\frac{E_\pi}{2\times10^{14}\,{\rm eV}}\right)^2\left(\frac{B}{10^6\,{\rm G}}\right)\ {\rm eV}. \quad (14)$$

Thus, pions of 10^{14}–10^{15} eV emit photons of 10^7–10^9 eV. The energy of muon synchrotron radiation is distributed mainly in the range of 10^5–10^7 eV. The conversion efficiency into high-energy photons in the cascade process is fairly large, much larger than that into neutrinos.

In the Continuous Model, since the magnetic field is weaker, the synchrotron cooling time scale becomes longer, comparable to the decay time for charged pions with energy of 10^{15} eV. In a similar way to that in the Discrete Model, we obtain $m_\pi c^2\gamma_{\pi^0} \simeq 5\times10^{14}(f_{\rm B}/0.1)^{-1/2}\eta_2^{-2}L_{52}^{-1/2}\mathcal{R}$ eV, which is slightly larger than $E_{{\rm p},\tau}$. However, the synchrotron cooling time of muons is still shorter than the decay time scale for the relevant energy range. Thus, the conversion efficiency into high-energy photons is still large in the Continuous Model, too.

2.4. Electron–Positron Pair Production

As was argued in subsection 2.3, a large fraction of the energy of accelerated protons is converted into high-energy photons both in the Discrete and Continuous Models. Typical energies of photons from neutral pions are above 10^{13} eV while those from charged pions and muons are below 10^9 eV. The high-energy photons emitted from π^0s and $\pi^{\pm}$s create electron–positron pairs through collisions with residual thermal photons. The cross section of the pair creation is written as $\sigma_\pm = \sigma_{\rm T} g(y)$ (Berestetskii et al. 1982), where

$$g(y) = \frac{3}{16}(1-y^2)\left[(3-y^4)\ln\frac{1+y}{1-y} - 2y(2-y^2)\right]. \quad (15)$$

The dimensionless value y is defined by $y^2 = 1 - (2m_{\rm e}^2c^4)/[\varepsilon_\gamma\varepsilon'_\gamma(1-\cos\theta)]$. In figure 6, we plot the time scale and the optical depth ($\tau_{\gamma\gamma}$) against the pair creation in the 100 eV radiation field for the Discrete Model. Figure 6 shows that the photons with energy from $\varepsilon_\gamma = 3\times10^8$ eV to 4×10^{14} eV create electron–positron pairs before they escape from the shell with $l = 10^9$ cm. We define the threshold energy ε_τ, above which photons create pairs. Photons from the decay of neutral pions and high-energy part of the synchrotron radiation from charged pions can be converted into pairs, while low-energy synchrotron photons will directly escape.

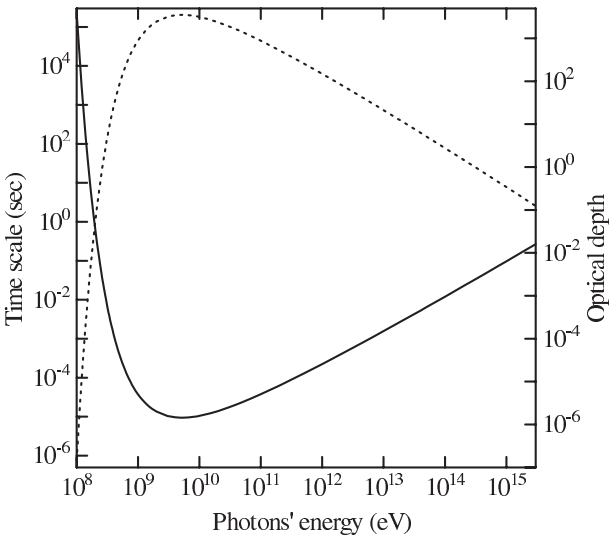

Fig. 6. Time scale (solid line) and the optical depth (dotted line) of photons for the pair creation in the thermal photon field. We assume $T = 100$ eV and $l = 10^9$ cm in this figure.

In the Continuous Model, ε_τ turns out to be similar, since the larger available size compensates for the smaller photon density, which results in a similar value of $\tau_{\gamma\gamma}$. Since both models give a similar input of high-energy photons, and a similar optical thickness to the pair absorption, the subsequent development of the cascade is also similar.

First we consider pair production of photons from decay of the neutral pions. Such electrons and positrons emit the synchrotron radiation, the energy of which is given by

$$\frac{\hbar q B}{m_{\rm e}c}\gamma_\pm^2 \sim 4\left(\frac{B}{10^6\,{\rm G}}\right)\left(\frac{\gamma_\pm m_{\rm e}c^2}{10^{10}\,{\rm eV}}\right)^2\ {\rm MeV}, \quad (16)$$

where $\gamma_\pm$ is the Lorentz factor of the pairs. Since the quantum effect is important for electrons higher than 10^{13} eV for $B = 10^6$ G, the emitted energy is comparable to the energy

of the emitter themselves. Those photons create pairs again. Reiterating the pair creation and the synchrotron radiation, these high-energy photons cascade into low-energy pairs.

The energy of electrons/positrons which emit photons with a critical energy of $\varepsilon_\tau = 3 \times 10^8$ eV is 8×10^{10} eV. Thus, the synchrotron photons emitted from electron/positrons above 8×10^{10} eV are absorbed through pair production, while those emitted by pairs below 8×10^{10} eV escape from the shell. Thus, for $m_e c^2 \gamma_\pm \geq \varepsilon_\tau = 3 \times 10^8$ eV, the injection of pairs due to pair absorption of synchrotron photons emitted from higher energy pairs balancing with synchrotron cooling makes the resultant number spectrum of pairs as steep as $N_\pm \propto \gamma_\pm^{-3}$. On the other hand, below 3×10^8 eV, pair injection becomes unimportant, and the number spectrum of pairs is determined only by radiative cooling as $N_\pm \propto \gamma_\pm^{-2}$. Then, the typical energy of the synchrotron emission from pairs with break energy $\varepsilon_\tau = 3 \times 10^8$ eV is

$$\varepsilon_\pm = \frac{\hbar q B}{m_e c} \left(\frac{\varepsilon_\tau}{m_e c^2} \right)^2 \sim 4 \left(\frac{B}{10^6\,\mathrm{G}} \right) \ \mathrm{keV}. \tag{17}$$

As a result, the photon index of synchrotron radiation becomes -2 above $\varepsilon_\pm$, while below that the photon index becomes -1.5. Since the energy of photons will be blue-shifted by the relativistic motion of the shocked shell [$\Gamma_m \simeq \Gamma_r(\Gamma_R - \sqrt{\Gamma_R^2 - 1}) \sim 200$], this typical energy is observed as a few hundred keV, which is consistent with the observations.

In the Continuous Model, similar processes are generated, and the main differences lie in the behavior of B and $\tau_{\gamma\gamma}$ as a function of r. In figure 7 we plot the typical photon energy $\varepsilon_\pm$ emitted from the pairs of typical energy ε_τ against r. Here, we have assumed $\eta_2 = 1$, $\Delta_7 = 1$, and $f_B = 0.1$. The value $\varepsilon_\pm$ has been calculated for radii where the photopion production can occur by the thermal radiation field. Since ε_τ does not change very much against the change in the optical depth, $\varepsilon_\pm$ practically behaves as $\propto B \propto r^{-1}$ in figure 7. The value $\varepsilon_\pm$ is around 0.1–10 keV in the wind frame, which is typically observed as 0.01–1 MeV, similar to the Discrete Model. Thus, the results in the Discrete and Continuous Models are basically the same. In both models the gamma-ray emission can be ignited by photopion production against the residual radiation field.

Next, we consider the fate of synchrotron photons emitted by charged pions and muons. Since the energy range is typically 10^5–10^9 eV, only the high-energy portion of the spectrum is absorbed and produce pairs at around $\varepsilon_\tau = 3 \times 10^8$ eV, while the lower energy photons directly escape. Thus, around the break energy, synchrotron radiation of pairs originating from charged pions superposes on the smoother component of cascades from neutral pions.

It is to be noted that this is not the whole story because the thus-produced photons overweigh the residual photons and modify the cascading behavior itself. Thus, we expect that the optical thickness to the pair absorption drastically increases and that lower energy photons which have been regarded to directly escape in the above will also be pair-absorbed to enhance the cascade process.

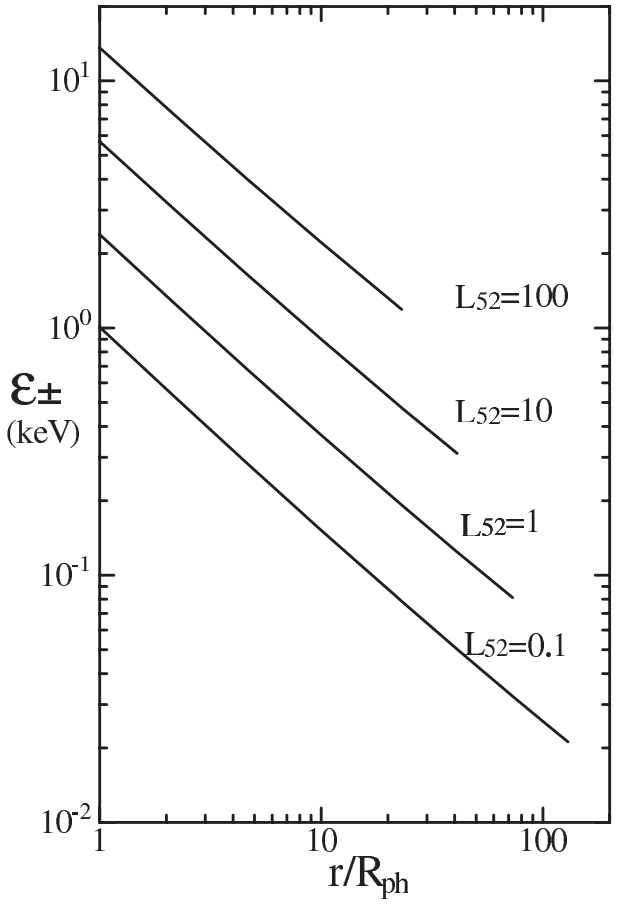

Fig. 7. Photon energy $\varepsilon_\pm$ in the comoving frame for $\eta_2 = 1$ and $\Delta_7 = 1$ in Continuous Model.

3. Emission from Cascading Particles

As discussed in section 2, the residual radiation field of the fireball can trigger a cascade from shock-accelerated relativistic protons. The photon field from the cascading particles itself will overwhelm the thermal radiation field as the cascade process goes on, and the cascade process proceeds nonlinearly. The energy density of the photons generated in the cascades is larger than that of the residual photons by about one order of magnitude. In this section we discuss the effects of the self-generated photon field on the resultant emission spectra.

3.1. Self-Generated Photon Field

Self-generated photons drastically decrease the threshold energy of pair creation (ε_τ) and make inverse Compton scattering as important as the synchrotron radiation as the cooling processes of pairs. The cascade process proceeds as shown in figure 8. Although the whole process is time-dependent, we here treat effects of these photons within the steady state one-zone model. In the Discrete Model, for simplicity, we assume that the fraction f_γ of the internal energy U_{in} in the shocked shell goes into the radiation field, and the photon number density obeys a power-law distribution as

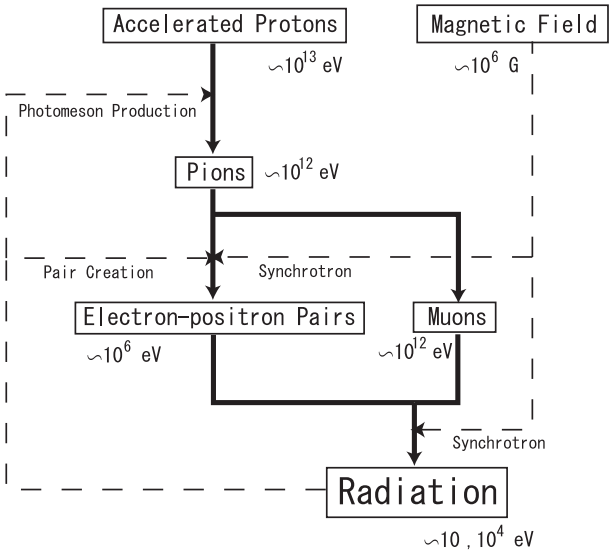

Fig. 8. Emission process when the photon field due to the cascading particles itself overwhelms the residual radiation (see section 3). The notation is the same as in figure 1.

$$n(\varepsilon_\gamma) = (\alpha-2)\frac{f_\gamma U_{\rm in}}{\varepsilon_0^2}\begin{cases} \left(\varepsilon_\gamma/\varepsilon_0\right)^{-\alpha} & (\text{for} \quad \varepsilon_\gamma > \varepsilon_0) \\ 0 & (\text{for} \quad \varepsilon_\gamma \le \varepsilon_0). \end{cases} \tag{18}$$

Of course, this photon spectrum will not generally be coincident with the radiation field that is finally realized. As shown below, however, the typical energy of the cascading particles is not very sensitive to the shape of the photon spectra, but is determined mainly by f_γ.

In the Continuous Model we assume that the photon density is similarly obtained using U in equation (8).

3.2. *Photopion Production*

For the photon field given by equation (18), τ_π is analytically obtained as

$$\tau_\pi(\gamma_{\rm p}) = Cf_\gamma 2^\alpha \frac{\alpha-2}{\alpha+1}\frac{\sigma_{\rm eff}(\alpha)}{\sigma_{\rm T}}\frac{m_{\rm p}c^2}{\varepsilon_0}\left(\frac{\varepsilon_0\gamma_{\rm p}}{m_{\rm e}c^2}\right)^{\alpha-1}, \tag{19}$$

where $\sigma_{\rm eff}(\alpha) \equiv \int d\chi\, \chi^{-\alpha}\sigma_\pi(\chi)$ and $\sigma_{\rm eff}(2.2) \simeq 2\times10^{-31}\,{\rm cm}^2$. The dimensionless factor C for the Discrete and Continuous Models becomes $\Gamma_{\rm R}-1$ and $\mathcal{R}^{-1}$, respectively. It is noted that the expression is independent of the parameters M and Δ etc., because we have normalized the physical values at $r = R_{\rm ph}$.

Since the threshold energy $E_{{\rm p},\tau}$ for which $\tau_\pi = 1$ has a dependence of $E_{{\rm p},\tau} \propto \varepsilon_0^{(2-\alpha)/(\alpha-1)}$, it turns out to be almost independent of ε_0 as long as $\alpha \simeq 2$. For $\alpha = 2.2$ and $\varepsilon_0 = 1\,{\rm keV}$, all protons for which energy is larger than

$$E_{{\rm p},\tau} = 10^{13}\left(\frac{Cf_\gamma}{0.3}\right)^{-5/6}\ {\rm eV}, \tag{20}$$

produce photopions. The threshold energy becomes an order of magnitude lower than in the previous section. Thus, the self-generated power-law photon field enhances the energy transfer from accelerated protons to photons and leptons. Since the inelasticity is about 0.2, the energy range of produced pions becomes 10^{12}–$10^{16}\,{\rm eV}$.

3.3. *Photon–Photon Pair Absorption*

The optical depth to the pair creation for a photon with energy ε_γ in the photon field given by equation (18) is analytically obtained as

$$\tau_{\gamma\gamma}(\varepsilon_\gamma) = Cf_\gamma F(\alpha)\frac{m_{\rm p}c^2}{\varepsilon_0}\left(\frac{\varepsilon_0\varepsilon_\gamma}{m_{\rm e}^2c^4}\right)^{\alpha-1}, \tag{21}$$

where

$$F(\alpha) = \frac{4(\alpha-2)}{\alpha+1}\int_0^1 dy\, y(1-y^2)^{\alpha-2}g(y) \tag{22}$$

is a dimensionless function [$F(2.2) \simeq 2\times10^{-2}$].

If $f_\gamma \simeq 0.3$, photons with energy $\gtrsim 1\,{\rm MeV}$ suffer from pair absorption, and do not directly escape from the shell. Thus, the pair cascade fully develops over the whole energy region of relativistic pairs. Synchrotron photons emitted from relativistic pairs distribute continuously over a wide energy range down to $\sim 0.01\,{\rm eV}$ without any significant breaks. In the observer frame this energy is blue-shifted to a few eV, which is much less than the observed break energy. In the Continuous Model, since $\tau_{\gamma\gamma} \propto r^{-1}$, the threshold energy ε_τ increases with r. However, the break energy of the synchrotron radiation does not become large enough because the magnetic field strength also decreases with r. Even for $r = 100R_{\rm ph}$ with the fiducial parameters, $\varepsilon_\tau \sim 10\,{\rm MeV}$ and $\varepsilon_\pm \sim 0.01\,{\rm eV}$ in the comoving frame.

Before we discuss the detailed behavior of the cascade, we examine if photons from pions have energies above $\sim 1\,{\rm MeV}$.

3.4. *Photons from Pions and Muons*

The produced π^0s promptly decay into two gamma-rays. As is the case of the residual thermal photon field, these photons with energy above $\sim 10^{12}\,{\rm eV}$ cascade into lower energy pairs.

As for the charged pions, high-energy pions cool through Compton and synchrotron radiation before decaying into muons, although Compton cooling is fairly suppressed by the Klein–Nishina effect in this energy range. In a similar way to that discussed in subsection 2.3, we obtain the Lorentz factor of pions, γ_{π^0}, whose lifetime is comparable to the cooling time as

$$\gamma_{\pi^0}^2 = \frac{3m_\pi c}{4t_{\pi,0}}\frac{\mathcal{L}}{(f_\gamma + f_{\rm B})m_{\rm p}c^2}\left(\frac{m_\pi}{m_{\rm e}}\right)^2, \tag{23}$$

where the length scale $\mathcal{L}$ for the Discrete and Continuous Models becomes $l/(\Gamma_{\rm R}-1)$ and $R_{\rm ph}\mathcal{R}^2/\eta$, respectively. We should note that the typical value of $\mathcal{L}$ ($\sim 10^{11}\,{\rm cm}$) in the Continuous Model is much larger than that ($\sim 10^9\,{\rm cm}$) in the Discrete Model. The pions, whose energy is larger than $\gamma_{\pi^0}m_\pi c^2 \simeq 2\times10^{13}(\mathcal{L}/10^9\,{\rm cm})^{1/2}[(f_\gamma+f_{\rm B})/0.4]^{-1/2}\,{\rm eV}$, should cool down before they decay into muons and neutrinos. According to equation (14), synchrotron photons from charged pions above $3\times10^{13}\,{\rm eV}$ suffer from pair absorption, while those from charged pions below $3\times10^{13}\,{\rm eV}$ do not. Thus, a major portion of the energy of high-energy charged pions will be injected into the cascade process, and some part results in the emission of photons in the sub-MeV range.

Although charged pions below $\sim 10^{13}\,{\rm eV}$ decay into muons and neutrinos before significant radiative cooling, the muons

take a large fraction ($\sim m_\mu/m_\pi \sim 0.8$) of the original energy of pions and contribute to photon emission. Muons cool down through the synchrotron and inverse Compton mechanisms. As is seen when we estimate γ_{π^0}, it turns out that the muons, whose energy is larger than $\gamma_{\mu^0} m_\mu c^2 \sim 10^{12}(\mathcal{L}/10^9\,\mathrm{cm})^{1/2}[(f_\gamma + f_\mathrm{B})/0.4]^{-1/2}\,\mathrm{eV}$, should cool down before they decay into electrons. Since the Klein–Nishina suppression works for target photons of energy larger than 10 keV, we should take this limit into account for f_γ. In the Discrete Model, since muons are injected in the energy range of $\sim 10^{12}$–$10^{13}\,\mathrm{eV}$, muons lose more than a half of the initial energy radiatively before decay. The cooling time is $t_{\mu,\mathrm{cool}} \simeq 0.03(\mathcal{L}/10^9\mathrm{cm})^{1/2}[(f_\gamma + f_\mathrm{B})/0.4]^{-1/2}$ s that is comparable to the dynamical time scale l/c.

The typical energy of muon synchrotron radiation is

$$\frac{\hbar q B}{m_\mu c}\gamma_{\mu^0}^2 = \frac{3\sqrt{2\pi}\hbar q}{2t_{\mu,0}}\frac{f_\mathrm{B}^{1/2}}{f_\gamma + f_\mathrm{B}}\sqrt{\frac{\mathcal{L}}{m_\mathrm{p}c^2\sigma_\mathrm{T}}} \tag{24}$$

$$\simeq 20\left(\frac{f_\mathrm{B}}{0.1}\right)^{1/2}\left(\frac{f_\gamma + f_\mathrm{B}}{0.4}\right)^{-1}\left(\frac{\mathcal{L}}{10^9\,\mathrm{cm}}\right)^{1/2}\mathrm{keV}. \tag{25}$$

This energy should be blue-shifted by the relativistic motion of the shocked shell ($\Gamma_\mathrm{m} \sim 200$) and observed as $\sim$ MeV, which is slightly higher than the observed break energy of GRBs. The synchrotron spectrum from muon cooling is broadly concentrated around the above typical energy. The muons, whose energy is smaller than $\gamma_{\mu^0} m_\mu c^2$, decay into electrons. These electrons emit very high-energy photons that cannot escape from the shell because of pair absorption.

In the Continuous Model, since $\mathcal{L} \sim 10^{11}\,\mathrm{cm}$, the typical energy of muon synchrotron becomes an order of magnitude larger than in the Discrete Model.

3.5. Pair Cascade

In the cascade process, as long as the energy density of power law photons is comparable to that of the magnetic field, the Compton scattering also produces high-energy photons, although Klein–Nishina suppression is significant in the high-energy regime. As the energy of pairs in the cascade process decreases, the Compton scattering plays a major role. In addition, created pairs increase the optical thickness to the scattering. These processes may modify the resultant spectrum. In order to obtain the detailed spectrum in the pair-cascade model we need to simulate electron–positron plasmas including the effects of synchrotron radiation, Compton scattering, pair creation, pair annihilation, Coulomb scattering, e–e bremsstrahlung, and so on. However, such numerical calculation is beyond the scope of this paper.

Here, we qualitatively discuss the spectrum emitted from cascading pairs, especially the possible breaks in the spectrum. We simply estimate the prospective physical conditions of the plasmas with the help of published numerical simulations made for pair cascade models for compact X-ray sources (Guilbert et al. 1983; Lightman, Zdziarski 1987; Coppi 1992; Stern et al. 1995). These previous simulations assumed that copious soft photons are injected at lower energies, which correspond to the residual thermal photons of the fireball in the present case. In the present case, the magnetic field is relatively large; its energy density is comparable to that of injected high-energy photons.

In terms of the compactness parameter, our case corresponds to

$$l_\mathrm{e} \equiv \frac{L_\pi \sigma_\mathrm{T}}{l m_\mathrm{e} c^3} = C f_\pm \frac{m_\mathrm{p}}{m_\mathrm{e}} \simeq 550\left(\frac{C f_\pm}{0.3}\right), \tag{26}$$

where we have taken a volume l^3 because our case is not spherical. Although this typical value of the compactness parameter is somewhat large compared with those adopted in the above-mentioned studies, the qualitative features will not be different.

The created pairs above $\sim 1\,\mathrm{MeV}$ will distribute in a monotonic fashion. The pairs cool down mainly through synchrotron radiation and inverse Compton scattering to form a power-law spectrum with a number index of around 3, as discussed in subsection 2.4. This corresponds to the case when all of the injected energy flows down in the energy space while making lower energy pairs and photons. The number spectra of synchrotron emission and inverse Compton scattering is described by a power law of index around 2. This very rough consideration is a fairly good approximation as the simulations with the power law injection of pairs by Coppi (1992) showed the power law indices of photons in the case of $f_\gamma \sim f_\mathrm{B}$ become around 2 in the range $x \equiv \varepsilon_\gamma/m_\mathrm{e}c^2 = 10^{-3}$–$10^{-1}$, which we are interested in. Below this energy, the effects of cooled pairs appear while above $x = 1$ the effects of pair absorption play a role.

As the low-energy pairs accumulate, a sharp break due to the synchrotron self-absorption appears in the spectrum in the case of $f_\mathrm{B} \simeq f_\gamma$. Assuming $N_\pm \propto \gamma_\pm^{-(p+1)}$ above $E_{\pm,\mathrm{min}}$, we obtain the synchrotron self-absorption frequency (Rybicki, Lightman 1979) as

$$\varepsilon_\mathrm{abs} \simeq 10\left(\frac{f_\gamma + f_\mathrm{B}}{0.4}\right)^{-0.28}\left(\frac{f_\pm}{0.3}\right)^{0.28}\left(\frac{f_\mathrm{B}}{0.1}\right)^{0.36} \times \left(\frac{\mathcal{L}}{10^9\mathrm{cm}}\right)^{-0.36}\left(\frac{E_{\pm,\mathrm{min}}}{1\,\mathrm{MeV}}\right)^{0.61}\mathrm{eV}, \tag{27}$$

for $p = 2.2$. The predicted self-absorption energy becomes $\sim 2\,\mathrm{keV}$ in the observer frame for $\Gamma_\mathrm{m} \simeq 200$, lower than the observed break energy.

Next we discuss the cooled pairs. Following the convention, we define the "pair yield" as $PY \equiv \int d\gamma_\pm P(\gamma_\pm) \,/\, \int d\gamma_\pm Q(\gamma_\pm)(\gamma_\pm - 1)$, where $Q(\gamma_\pm)$ is the rate of injection of pairs of $\gamma_\pm$ via the pion decay, and $P(\gamma_\pm)$ is the rate at which secondary pairs of $\gamma_\pm$ are created via pair production. Since the numerical simulations indicated that for $l_\mathrm{e} \gg 10$ the value PY becomes ~ 0.1 independent of other parameters, we assume $PY \simeq 0.1$ hereafter. This means that 10% of the injected energy goes into the rest mass energy of cooled pairs and the remaining 90% of energy goes into radiation. Created pairs may cool down to subrelativistic energies and thermalize before annihilating. In the steady state, the pair creation rate is assumed to balance with the rate of pair annihilation. We thus obtain

$$\frac{3}{8}\sigma_\mathrm{T} c n_+ n_- = \frac{1}{2}\int P(\gamma_\pm)\, d\gamma_\pm, \tag{28}$$

where n_+ and n_- are the number densities of cooled thermal positrons and electrons, respectively. The Thomson optical depth to thermal pairs is written by

$$\tau_\pm = \left(\frac{4}{\pi} l_e P Y\right)^{1/2} = 7 \left(\frac{C f_\pm}{0.3}\right)^{1/2} \left(\frac{PY}{0.1}\right)^{1/2}. \quad (29)$$

The equilibrium temperature of the thermal pairs, $T_\pm$, is mainly determined by requiring that no net energy be transferred between the particles and photons. Numerical simulations for compact X-ray sources in the past showed $\Theta \equiv T_\pm / m_e c^2 \sim 10^{-2}$–$10^{-3}$ for $l_e \gg 10$ regardless of the other parameters. Therefore, the Compton y parameter, $y \sim 4\Theta\tau_\pm^2 \lesssim 1$, in our model and relatively mild Comptonization may occur. The photon energy tends to be peaked around at 1–10 keV, which is expected for the observed break energy of GRBs when beaming effects are taken into account.

Because of the large Thomson optical depth of thermal pairs ($\tau_\pm$), the mean energy loss of photons with energy lower than $m_e c^2$ in one scattering by cold thermal pairs is about $\varepsilon_\gamma^2 / m_e c^2$, and the mean number of scattering is about $\tau_\pm^2$. A significant depletion of the spectrum may occur in the region $1/\tau_\pm^2 \lesssim x \lesssim 1$ (Lightman, Zdziarski 1987; Coppi 1992; Stern et al. 1995), due to downscattering of photons by cold thermal pairs. The break energy, $m_e c^2 / \tau_\pm^2 \simeq$ a few or a few tens of keV, can be the same order of observed break energy owing to the relativistic blue-shift. Thus, cooled thermal pairs may possibly produce spectral break compatible with observations through thermal Comptonization and downscattering of high-energy photons. However, in order to quantitatively investigate this possibility, detailed numerical simulations will be required.

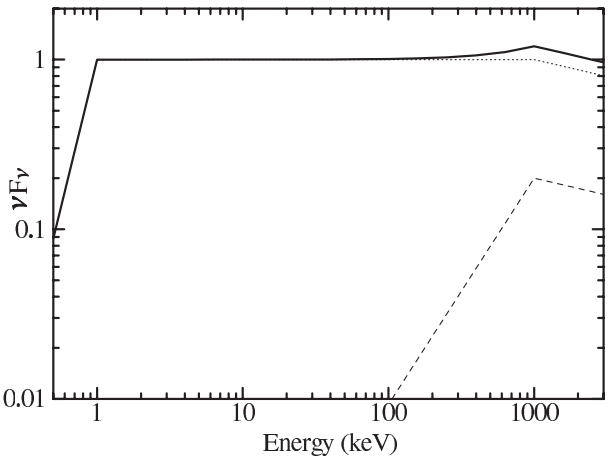

Fig. 9. Schematic photon spectrum in the observer frame. The dotted and dashed lines are the components due to the electron–positron pairs and muons, respectively. The solid line shows the integrated spectrum. Here, we assume that the energy of the component from the muons is much smaller than the energy of the component from the pairs. The break due to the self-absorption appears at ~ 1 keV. The downscattering by cold thermal pairs makes both the components above ~ 1 MeV decrease.

4. Discussion

We have shown that Fermi-accelerated protons with $\gtrsim 10^{13}$ eV efficiently bring their energy into pion production and subsequent photon emission. The photon spectra of the cascades from relativistic protons are mainly characterized by synchrotron and inverse Compton components emitted from pairs. In addition, muon synchrotron radiation can make an important contribution. Cooled thermal pairs can modify the photon spectra through Comptonization and downscattering of high-energy photons. In figure 9, we show the schematic spectra which we discussed above. Although we have discussed several mechanisms to reproduce the observed break energy scale including muon synchrotron radiation, synchrotron self-absorption, Comptonization, and downscattering by cooled thermal pairs, at present we have not definitely identified any specific one with the observed break feature. The problem remains to be open.

Let us briefly discuss this problem. The simplest way to produce a sharp spectral break is to prevent electrons/positrons from cascading below the typical energy, ε_τ. As discussed in section 2, if the photon density in the shocked region is sufficiently low, the pair-creation process cannot provide electron–positron pairs under energy ε_τ. The value of ε_τ should be large enough ($\sim 100 m_e c^2$) to reproduce the spectral break [see equation (17)]. However, the condition that the emission from the cascading particles themselves is more luminous than the residual radiation of the fireball implies $f_\gamma \gtrsim 0.1$ consistent with the value we have adopted in section 3. In addition, f_γ may be larger than ~ 0.1 to reproduce the energetics of GRBs. Thus, the condition $f_\gamma \gtrsim 0.1$ is universally required so that the pair cascade develops over the whole energy region of relativistic pairs (namely $\varepsilon_\tau \sim m_e c^2$).

As shown in figures 5 and 7, in the Continuous Model the cascade process can occur even far outside of R_{ph}. If internal shocks occur far beyond R_{ph}, the photon density is diluted and ε_τ can be large. As discussed in subsection 3.3, however, the smaller magnetic field prevents the break energy from increasing sufficiently.

We have neglected effects of the directly accelerated electrons. If the total energy of electrons directly accelerated is more than a tenth of the energy of the protons, the synchrotron emission from the electrons can make the ignition of photopion production easier. However, the emission from the electrons does not modify the cascade process very much. Therefore, even in this case ε_τ remains too small to reproduce the observed break energy.

One may think that the cascade process can be largely altered if $f_B \ll 0.1$. Here, we argue that this is not the case. As far as $B > 100$ G with $f_B \gtrsim 10^{-9}$, protons can be accelerated beyond 10^{13} eV for $l = 10^9$ cm and photopion production against residual photons occurs efficiently. While synchrotron cooling of charged pions is strongly suppressed, neutral pions decay into two gamma-rays and create electron–positron pairs through collisions with residual thermal photons. The energy of those pairs is comparable to the energy of π^0s ($\sim 10^{13}$ eV). Even though the Klein–Nishina suppression makes inverse Compton process ineffective for such pairs, the pairs cool down through synchrotron radiation; even for $B = 100$ G the cooling time of pairs via synchrotron radiation is shorter than the dynamical time scale because of their large Lorentz factor. The energy of synchrotron photons emitted from the pairs is larger than

100 MeV for $B \geq 100$ G. Therefore, the synchrotron photons create secondary pairs again (see subsection 2.4) and the energy of π^0s is transfered to lower energy pairs via the cascade process illustrated above. The low energy pairs cool through inverse Compton process against residual photons and produce the self-generated photon field. When the self-generated photons overwhelm the residual photons ($f_\gamma \gtrsim 0.01$), the cooling processes of low-energy pairs, charged pions, and muons are dominated by inverse Compton process, rather than synchrotron radiation. For $f_\gamma \gtrsim 0.1$ the values of γ_{π^0} [see equation (23)], γ_{μ^0}, and ε_τ remain close to the values for $f_B = 0.1$. Thus, even when $f_B \ll 0.1$, the cascade process proceeds in a similar way as discussed in section 3. Cooled muons with γ_{μ^0} decay and provide electrons/positrons within a narrow energy range around 10^{11} eV (see subsection 3.4). Photons emitted from such electrons/positrons can be in a narrow energy spectrum, and escape without producing pairs. Even for $B = 100$ G, the energy of the synchrotron photons emitted from the electrons of 10^{11} eV is 40 keV in the comoving frame. This energy is an order of magnitude larger than the typical break energy. Since the Klein–Nishina suppression is significant for such electrons/positrons, the cooling time also tends to be longer than the dynamical time scale. In any case, most of the self-generated photons come from neutral pions. The spectrum component due to the cascade process initiated from π^0-decay may not reproduce the break energy.

From the above discussion, pairs generally distribute over a wide energy range, which overpredicts the flux of low-energy photons between ~ 1 keV and ~ 1 MeV within a simple analysis. There may be no physical process to prevent electrons/positrons from cascading into lower energy. The possible mechanisms to make the spectral break may be Comptonization or downscattering of high-energy photons by cooled thermal pairs. It is difficult to estimate the precise effects of Comptonization and downscattering analytically. The Comptonization may resolve the problem of the spectral index below the break. We have assumed $f_B \sim f_\gamma$ in our discussion. A smaller value of f_B makes inverse Compton scattering dominant rather than synchrotron radiation. Some numerical simulations showed that the spectral index decreases with decreasing f_B/f_γ (Zdziarski, Lamb 1986; Coppi 1992). A smaller value of f_B is favorable to decrease the spectral index below the break. After all, we need to simulate the cascade and emission processes numerically to predict the final spectra quantitatively.

Our model may explain some puzzling features of GRBs. For example, some spectra obtained by the Ginga satellite show break energies of a few or a few ten keV and spectral number index smaller than 2 below the breaks (Strohmayer et al. 1998). These break energies are close to the self-absorption frequency in our model. Since the emission spectra in the X-ray and gamma-ray range should depend on details of the model parameters, such as the positions of the internal shock and photosphere, our model may provide a wide range of spectral and timing behavior. It is interesting to see if our model can reproduce not only the standard spectral feature, but also the anomalous spectrum, like the "X-ray rich GRB" (Heise et al. 2001; Kippen et al. 2001) or GRB precursor (Koshut et al. 1995).

Our scenario also predicts several features of neutrino emission. The cooling of muons and pions results in a clustering of neutrino energies. From the typical energy of pions at the decaying moment, we obtain the energy of ν_μ ($\bar{\nu}_\mu$), which is produced from the decay of π^+ (π^-) as $0.2\gamma_{\pi^0} m_\pi c^2 \Gamma_m \simeq 9 \times 10^{14} (\Gamma_m/200)$ eV in the observer frame. If f_γ and f_B are sufficiently small, the energy of neutrinos can be large. In this case, however, a small f_γ means a weak flux of neutrinos. The energy of ν_e and $\overline{\nu}_\mu$ ($\overline{\nu}_e$ and ν_μ), which is produced from the decay of μ^+ (μ^-), is as small as $\sim 7 \times 10^{13} (\Gamma_m/200)$ eV in the observer frame.

5. Conclusions

We have investigated the consequences of proton acceleration in the residual thermal photon field in the internal shocks of GRBs. Even if the internal energy of heated protons cannot be converted into the energy of electrons, radiation energy can be drained from the accelerated protons through the photopion production process against residual thermal photons. We have examined two extreme models concerning the distribution of residual thermal photons. In the Discrete Model, photons are confined within multiple thin shells, while in the Continuous Model, photons are emitted from the wind photosphere. In both the Discrete and Continuous Models the residual radiation field in the fireball is shown to be able to ignite the photopion production and the generated photon field further enhances the photon-initiated cascade. Although the real situation lies between these two extreme models, there are no large differences in the ignition processes. The Fermi-accelerated protons with $\gtrsim 10^{13}$ eV bring their energy into pions. If the number fraction ζ of protons are accelerated and distributed as $n_p \propto E_p^{-q}$, and if they have the fraction ξ of the internal energy, the energy fraction of pions is obtained by

$$f_\pi \simeq \left(\frac{q-2}{q-1}\right)^{q-2} \zeta^{2-q} \xi^{q-1} \left(\frac{E_{p,\tau}}{m_p c^2}\right)^{2-q} \tag{30}$$

$$= 0.3 \left(\frac{\zeta}{0.01\%}\right)^{-0.2} \left(\frac{\xi}{50\%}\right)^{1.2} \left(\frac{E_{p,\tau}}{10^{13}\,\mathrm{eV}}\right)^{-0.2}, \tag{31}$$

for $q = 2.2$.

The particles cascading from the pions emit photons over a wide energy range. The emission properties for the two models are also similar. The spectrum is composed of mainly two components: emissions from the electron–positron pairs and muons, produced by high-energy photons and charged pions, respectively. The pairs form a power-law spectrum with a number index of around 3 over the whole energy region of relativistic pairs. On the other hand muons cool down to a characteristic energy before they decay. The radiation due to the pairs is composed of a power-law spectrum with an index of about 2 with possible break features around the 1–10 keV range in the comoving frame due to Comptonization and downscattering by cooled thermal pairs. This may correspond to the observed break when the relativistic beaming effects are taken into account. The muons can emit X- and gamma-rays by synchrotron process and produce a sharp break at around 1–10 MeV in the spectrum.

This work is supported in part by a Grant-in-Aid for Scientific Research from the Japanese Ministry of Education, Culture, Sports, Science and Technology (No. 13440061, F.T.). One of the authors (K.A.) was supported by the Japan Society for the Promotion of Science.

References

Berestetskii, V. B., Lifshitz, E. M., & Pitaevskii, L. P. 1982, Quantum Electrodynamics (New York: Pergamon), p. 371
Coppi, P. S. 1992, MNRAS, 258, 657
Goodman, J. 1986, ApJ, 308, L47
Guetta, D., Spada, M., & Waxman, E. 2001, ApJ, 557, 399
Guilbert, P. W., Fabian, A. C., & Rees, M. J. 1983, MNRAS, 205, 593
Heise, J., in 't Zand, J., Kippen, R. M., & Woods, P. M. 2001, in ESO Astrophysics Symposia: Gamma-ray Bursts in the Afterglow Era, ed. E. Costa, F. Frontera, & J. Hjorth (Berlin: Springer), 16
Kippen, R. M., Woods, P. M., Heise, J., in 't Zand, J., Preece, R. D., & Briggs, M. S. 2001, in ESO Astrophysics Symposia: Gamma-ray Bursts in the Afterglow Era, ed. E. Costa, F. Frontera, & J. Hjorth (Berlin: Springer), 22
Kobayashi, S., & Sari, R. 2001, ApJ, 551, 934
Koshut, T. M., Kouveliotou, C., Paciesas, W. S., van Paradijs, J., Pendleton, G. N., Briggs, M. S., Fishman, G. J., & Meegan, C. A. 1995, ApJ, 452, 145
Lightman, A. P., & Zdziarski, A. A. 1987, ApJ, 319, 643
Medvedev, M. V., & Loeb, A. 1999, ApJ, 526, 697
Mészáros, P., & Rees, M. J. 1993, ApJ, 405, 278
Mészáros, P., & Rees, M. J. 2000, ApJ, 530, 292
Paczyński, B. 1986, ApJ, 308, L43
Piran, T. 1999, Phys. Rep., 314, 575
Piran, T., Shemi, A., & Narayan, R. 1993, MNRAS, 263, 861
Preece, R. D., Briggs, M. S., Mallozzi, R. S., Pendleton, G. N., Paciesas, W. S., & Band, D. L. 1998, ApJ, 506, L23
Preece, R. D., Briggs, M. S., Mallozzi, R. S., Pendleton, G. N., Paciesas, W. S., & Band, D. L. 2000, ApJS, 126, 19
Rees, M. J., & Mészáros, P. 1992, MNRAS, 258, 41p
Rybicki, G. B., & Lightman, A. P. 1979, Radiative Processes in Astrophysics (New York: Wiley-Interscience), p. 190
Sari, R., & Piran, T. 1995, ApJ, 455, L143
Shemi, A., & Piran, T. 1990, ApJ, 365, L55
Stecker, F. W. 1968, Phys. Rev. Lett., 21, 1016
Stern, B. E., Begelman, M. C., Sikora, M., & Svensson, R. 1995, MNRAS, 272, 291
Strohmayer, T. E., Fenimore, E. E., Murakami, T., & Yoshida, A. 1998, ApJ, 500, 873
Totani, T. 1999, MNRAS, 307, L41
Waxman, E. 1995, Phys. Rev. Lett., 75, 386
Waxman, E., & Bahcall, J. 1997, Phys. Rev. Lett., 78, 2292
Zdziarski, A. A., & Lamb, D. Q. 1986, ApJ, 309, L79